Stem Cell Reports
Article

OPEN ACCESS

HuCNS-SC Human NSCs Fail to Differentiate, Form Ectopic Clusters, and Provide No Cognitive Benefits in a Transgenic Model of Alzheimer's Disease

Samuel E. Marsh,[1,2,3] Stephen T. Yeung,[3] Maria Torres,[3] Lydia Lau,[3] Joy L. Davis,[3] Edwin S. Monuki,[2,3,4] Wayne W. Poon,[3] and Mathew Blurton-Jones[1,2,3,*]

[1]Department of Neurobiology & Behavior
[2]Sue & Bill Gross Stem Cell Research Center
[3]Institute for Memory Impairments & Neurological Disorders
[4]Department of Pathology & Laboratory Medicine
University of California Irvine, 845 Health Sciences Road, 3200 Gross Hall, Irvine, CA 92697, USA
*Correspondence: mblurton@uci.edu
http://dx.doi.org/10.1016/j.stemcr.2016.12.019

SUMMARY

Transplantation of neural stem cells (NSCs) can improve cognition in animal models of Alzheimer's disease (AD). However, AD is a protracted disorder, and prior studies have examined only short-term effects. We therefore used an immune-deficient model of AD (Rag-5xfAD mice) to examine long-term transplantation of human NSCs (StemCells Inc.; HuCNS-SCs). Five months after transplantation, HuCNS-SCs had engrafted and migrated throughout the hippocampus and exhibited no differences in survival or migration in response to β-amyloid pathology. Despite robust engraftment, HuCNS-SCs failed to terminally differentiate and over a quarter of the animals exhibited ectopic human cell clusters within the lateral ventricle. Unlike prior short-term experiments with research-grade HuCNS-SCs, we also found no evidence of improved cognition, no changes in brain-derived neurotrophic factor, and no increase in synaptic density. These data, while disappointing, reinforce the notion that individual human NSC lines need to be carefully assessed for efficacy and safety in appropriate long-term models.

INTRODUCTION

Alzheimer's disease (AD) is the most common cause of neurodegeneration, affecting over 35 million people worldwide (Alzheimer's Association, 2016). AD is a debilitating and progressive disease characterized by loss of memory, reasoning, and other cognitive functions that eventually robs patients of the ability to perform basic daily activities (Alzheimer's Association, 2016). Currently approved therapies provide only short-term palliative benefit and fail to modify disease pathology (Alzheimer's Association, 2016). Thus, there is an urgent need to identify novel and effective therapies for AD. Many preclinical and clinical studies have focused on reducing the accumulation of β-amyloid (Aβ), generally considered the most upstream cause of AD, which in turn induces hyperphosphorylation of tau, synaptic loss, and inflammation. However, thus far these anti-amyloid efforts have failed to slow cognitive decline in late-stage clinical trials (Schenk et al., 2012), although whether earlier intervention can provide efficacy is currently being examined (Sevigny et al., 2016).

While AD was initially considered too diffuse a disorder to benefit from neural stem cell (NSC) transplantation, recent studies have suggested that this may not be the case. For example, evidence from our laboratory and many others has shown that mouse NSCs (mNSCs) transplanted into a variety of different animal models, including models of Aβ accumulation, tauopathy, and neuronal loss, can improve cognition, enhance synaptic plasticity, and in some cases even modify pathology (Yamasaki et al., 2007; Blurton-Jones et al., 2009; Ryu et al., 2009; Hampton et al., 2010; Njie et al., 2012; Blurton-Jones et al., 2014). These studies, as well as research on other neurodegenerative diseases, have found that the therapeutic benefits of mNSC transplantation can often be attributed to neurotrophic-mediated increases in synaptic plasticity or mitigation of neuronal loss via secretion of neurotrophins such as brain-derived neurotrophic factor (BDNF) and glial cell line-derived neurotrophic factor (GDNF; Suzuki et al., 2007; Ebert et al., 2008; Blurton-Jones et al., 2009; Hampton et al., 2010; Goldberg et al., 2015). For example, we previously showed that short hairpin RNA (shRNA)-mediated reduction of BDNF within mNSCs abrogated the cognitive and synaptic benefits of mNSC transplantation in the 3xTg-AD model of AD (Blurton-Jones et al., 2009).

Thus far, the results from these mNSC transplantation studies for AD appear promising; however, it is important to now extend this line of inquiry to investigate the long-term safety and efficacy of human NSCs (hNSCs). As a first step in determining the translational potential of hNSCs, we recently examined the short-term efficacy of StemCells, Inc.'s research-grade fetal-derived hNSCs (HuCNS-SCs). One month after transplantation in immune-suppressed mouse models of AD (transgenic 3xTg-AD mice and hippocampal neuronal loss; Cam/Tet-DTA mice), we found that HuCNS-SCs improved cognitive function by enhancing axonal growth and synaptic connectivity (Ager et al., 2015). While these results again suggested that NSC transplantation could offer a promising approach, we sought to perform a follow-up study to address two important

questions. First, as AD is a protracted disorder and patients typically live 8–12 years after the initial diagnosis (Alzheimer's Association, 2016), it is critical to examine the long-term safety and efficacy of hNSC transplantation. Second, while our initial studies utilized a research-grade HuCNS-SC line, that line would not be applicable for patient use. We therefore sought to test a more clinically relevant HuCNS-SC line that was originally derived under good manufacturing practice (GMP) conditions.

Long-term xenotransplantation presents a significant technical challenge as drug and antibody-based immune suppression paradigms typically allow only about 3 months of xenograft survival before issues of toxicity and/or graft rejection occur, and many pharmaceutical immunosuppressants can independently modify AD pathology (Mollison et al., 1998; Taglialatela et al., 2009; Rozkalne et al., 2011; Anderson et al., 2011). In part to address these challenges and to study the influence of adaptive immunity on AD, we recently generated an immune-deficient transgenic model of AD by backcrossing the well-established 5xfAD transgenic mouse model (Oakley et al., 2006) onto a Rag2/il2rγ double-knockout background. The resulting mice lack T cells, B cells, and natural killer cells, the primary immune components responsible for the rejection of foreign cells, yet they develop extensive Aβ pathology (Marsh et al., 2016).

In the present study, we utilized this new model and observed that HuCNS-SCs survived for 5 months and migrated throughout the hippocampus. However, despite robust engraftment, transplanted HuCNS-SCs failed to terminally differentiate, decreased hippocampal synaptic density, produced no improvements in cognitive function, and had no effect on BDNF expression. Furthermore, HuCNS-SCs formed ectopic ventricular clusters in over a quarter of transplanted mice. These results with HuCNS-SCs that were originally derived under GMP conditions are in contrast to our previous report that utilized a research-grade HuCNS-SC line in a short-term model of AD. In the accompanying manuscript by Anderson et al. (2017), the authors report a similar lack of efficacy in a model of spinal cord injury between research-grade HuCNS-SCs and an "intended clinical cell lot/line" of HuCNS-SCs originally produced under GMP conditions. While disappointing, our results nevertheless highlight several important lessons broadly relevant to the development of NSC-based therapies and provide insight regarding the potential translational application of hNSCs for AD.

RESULTS

HuCNS-SCs

All derivation, maintenance, and passaging of HuCNS-SCs were performed by StemCells, Inc. HuCNS-SCs were derived as previously described (Uchida et al., 2000). Cells were initially generated, maintained, and passaged by StemCells, Inc. under GMP conditions. A vial of frozen passage 3 (P3) GMP cells was then transferred to the process development (PD) laboratory, which generated a bank of P6 cells. All previously described preclinical transplantations utilizing research-grade HuCNS-SCs were P8–P10 (Cummings et al., 2005; Sontag et al., 2014; Ager et al., 2015). The first batch of cells for the current study was generated in the PD laboratory, resulting in P10 cells, which, upon shipment to the University of California–Irvine, exhibited poor viability (~60%); they were therefore not used. Instead, additional frozen vials of P6 cells were transferred from the PD laboratory to StemCells, Inc.'s research laboratory and expanded to the same passage (P10) before overnight shipment. As the cells used in the current study were expanded from P3 to P10 outside of the GMP facility, they are not GMP grade. However, the design of the current study was to build from previous studies with research-grade HuCNS-SCs, which were derived and maintained in the research facility (Ager et al., 2015), by utilizing HuCNS-SCs initially derived under GMP conditions.

HuCNS-SC Survived and Migrated Extensively in the Rag-5xfAD Brain

Aβ can be toxic to many cell types; therefore, it is critical to empirically determine whether the accumulation and aggregation of Aβ can influence the long-term survival and engraftment of transplanted hNSCs. Rag-5xfAD mice provide an optimal model in which to test this question as they lack the key immune cells involved in xenogeneic cell rejection yet exhibit several hallmarks of AD pathogenesis, including robust amyloid accumulation, synaptic loss, and microgliosis (Marsh et al., 2016). To determine the survival and migratory capacity of fetal-derived HuCNS-SCs, bilateral hippocampal transplantation was performed (1×10^5 cells/side) at 2 months of age. HuCNS-SC survival and migration were subsequently quantified via unbiased stereology 5 months post-transplantation using the human-specific nuclear marker Ku80 (Figures 1A–1E). Five months post-transplantation, an average of 96,232 ± 5,394 cells, or 96.23%, survived and migrated in Rag-wild-type (WT) mice (n = 6). Surprisingly, Rag-5xfAD mice (n = 10) showed a nearly identical hNSC survival (90,265 ± 12,861, or 90.27%; p = 0.74).

HuCNS-SCs demonstrated excellent migratory capacity as cells were found throughout the entire rostral-caudal span of the hippocampus as well as in the corpus callosum, fimbria/fornix, subiculum, and some cortical regions (Figures 1F–1L; Movie S1). The migration of transplanted cells was indistinguishable between Rag-5xfAD and Rag-WT mice; HuCNS-SCs migrated up to ±1.713 mm (Rag-WT) and ±1.736 mm (Rag-5xfAD) from the hippocampal injection site.

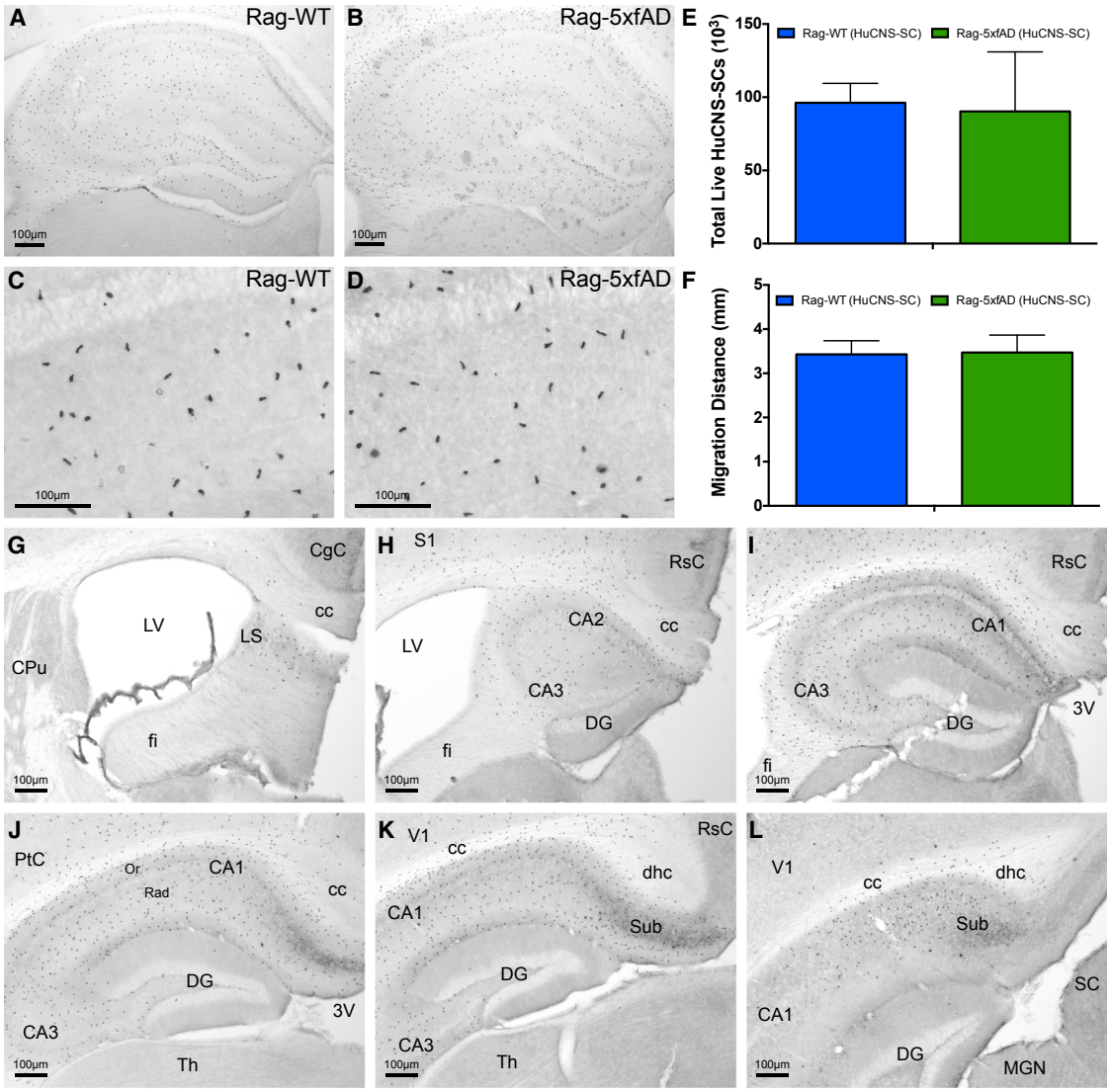

Figure 1. HuCNS-SCs Engraft and Migrate Equally Well in AD and Wild-Type Immune-Deficient Mice

(A–D) HuCNS-SCs (Ku80: human-specific nuclear marker) exhibit robust survival and migration throughout the rostral-caudal extent of the hippocampus in Rag-WT (A, C) and Rag-5xfAD mice (B, D).

(E and F) Unbiased stereological analysis of HuCNS-SC engraftment reveals no significant differences in total engrafted cells (E) or anterior-posterior (A/P) migration distance (F). Data presented as means ± SEM. N ≥ 8 mice/group.

(G–L) Representative images illustrating A/P migration of HuCNS-SC throughout hippocampal formation.

3V, third ventricle; CA1, field CA1 of the hippocampus; CA2, field CA2 of the hippocampus; CA3, field CA3 of the hippocampus; cc, corpus callosum; CgC, cingulate cortex; CPu, caudate putamen (striatum); DG, dentate gyrus; dhc, dorsal hippocampal commissure; fi, fimbria; LS, lateral septal nucleus; LV, lateral ventricle; MGN, medial geniculate nucleus; Or, oriens layer of the hippocampus; PtC, parietal cortex; Rad, radiatum layer of the hippocampus; RSC, retrosplenial cortex; S1, primary somatosensory cortex; SC, superior colliculus; Sub, subiculum; Th, thalamus; V1, primary visual cortex.

Scale bar, 100 μm. See also Movie S1.

HuCNS-SC Failed to Terminally Differentiate 5 Months Post-transplantation

To examine the differentiation of HuCNS-SCs, several multi-label immunohistological experiments were performed. Surprisingly, analysis of differentiation revealed that none of the intraparenchymally localized HuCNS-SCs expressed markers of mature terminal differentiation characteristic of the three potential neural lineages: neurons, oligodendrocytes, or astrocytes. No HuCNS-SCs were detected that expressed the mature neuronal marker

NeuN, the mature oligodendroglial marker APC (CC-1), or the astrocytic marker GFAP (Figures 2A–2I).

In contrast, virtually all HuCNS-SCs ($\geq$97.18% $\pm$ $\leq$0.80%) located within the brain parenchyma co-expressed doublecortin (DCX; Figures 2J–2L and 2S), a marker of immature neurons (Zhao et al., 2008), with no difference observed between Rag-WT and Rag-5xfAD genotypes (Figure 2S). Intriguingly, virtually all ($\geq$99.07% $\pm$ $\leq$0.35%) intraparenchymal HuCNS-SCs were also positive for Olig2 (Figures 2M–2O and 2S), a marker of immature and mature oligodendrocytes, which can also label immature astrocytes and multipotent progenitors (Jiang et al., 2013; Wang et al., 2013). Finally, none of the HuCNS-SCs within the brain parenchyma expressed human vimentin (Figures 2P–2R), seemingly ruling out immature astrocytic differentiation (Laywell et al., 2000). Thus, it appears that HuCNS-SCs failed to terminally differentiate, remaining relatively immature over the course of 5 months of engraftment.

Over a Quarter of Animals Exhibit Ectopic Clusters of HuCNS-SC Donor Cells within the Lateral Ventricle

During stereological quantification, human Ku80+ cell clusters were detected within the most rostral aspect of the lateral ventricle in over a quarter of all transplanted animals (3/10 Rag-5xfAD and 2/8 Rag-WT; Figure 3). These five animals displayed no other abnormal characteristics in either behavioral or pathological analyses, and there was no evidence of off-target injection or ventricular entry by the needle. Ectopic cell clusters were identified in the anterior portion of the lateral ventricle (Figure 3), >1.5 mm more rostral than the farthest point of intraparenchymal hNSC migration (Figure S1). These cell clusters also displayed distinct marker expression profiles in comparison with parenchymally engrafted cells. Although these clusters were immunoreactive for DCX, similar to intraparenchymal cells (Figures 3A–3C), they were mostly negative for Olig2 (Figures S2A–S2C), in contrast to 99% of parenchymally localized cells, which strongly expressed Olig2. Furthermore, cell clusters were positive for several glial markers, including human vimentin, CD44, S100β, and GFAP (Figures 3D–3O). Similar to parenchymal HuCNS-SCs, cell clusters were negative for NeuN (Figures S2D–S2F). The cell clusters were also found to co-express LIN28 (Figures 3P–3R), a marker expressed by embryonic stem cells and to a lesser extent NSCs (Darr and Benvenisty, 2009; Kawahara et al., 2011; Cimadamore et al., 2013), which is also observed in some primitive neural ectodermal tumors (PNETs) and medulloblastomas (Picard et al., 2012; Rodini et al., 2012). To determine whether these donor-derived cell clusters exhibited evidence of continued proliferation, Ki67 labeling was performed, revealing a relatively small proportion of actively proliferating human cells (3.7%; Figures S2G–S2I).

In several animals, human cells and/or processes derived from the ectopic clusters were found to infiltrate the adjacent tissue. Projections emanating from hNSC clusters were observed reaching through the ventricle walls into the striatum (Figures 3F and 3I, white arrows). We also observed several other instances in which groups of HuCNS-SCs from the clusters had infiltrated through the ventricle walls and entered the surrounding tissue (Figures 3L, 3O, and 3R, yellow arrows; Movie S2). In a smaller pilot study, a second independent HuCNS-SC line was injected into the hippocampus of Rag-5xfAD (n = 4). This particular experiment was not designed for biochemical and behavioral analysis; however, given our findings with the larger study, we carefully examined the brains and again detected a similar human cell cluster within the lateral ventricle of one of the four transplanted mice.

Histopathology Examination by a Contract Research Organization

To carefully examine the characteristics of the clusters, and to determine whether there was any evidence of neoplastic transformation, StemCells, Inc. sponsored a histopathological examination of these sections by a contract research organization (CRO; Charles River Laboratories). One H&E-stained section from four of the five animals exhibiting ventricular clusters and a series of Ku80-stained sections from all five mice were carefully analyzed by a board-certified veterinary pathologist, and a final pathology report was generated. The report concluded "no evidence of neoplastic transformation is present" and that "no evidence of cellular pleomorphism, atypia, mitoses or invasion of the adjacent neuroparenchyma was present in the sections examined." One cluster exhibited a "small degree of nuclear size variation," but "no other cytomorphologic abnormalities were present."

While these conclusions were reassuring, we also asked a practicing board-certified human neuropathologist (E.S.M) to examine the same sections and images. While largely concurring with the descriptive CRO assessment, E.S.M. concluded that the intraparenchymal cells clearly displayed a phenotype distinct from the nodular intraventricular clusters, which had features reminiscent of central neurocytoma (see Discussion), and the data depicted in Figures 3 and S2, and Movie S2 were interpreted as infiltration into the adjacent parenchyma. However, the significance of these findings remains uncertain since normal HuCNS-SCs are expected to be highly migratory. Similarly, the nodular intraventricular pattern itself may reflect a "normal" NSC phenotype related to its distinct cell-cell and intraventricular environment rather than an oncogenic phenotype per se. Nonetheless, the repeated appearance of these clusters in multiple animals, their distance from the injection sites, location within the ventricle,

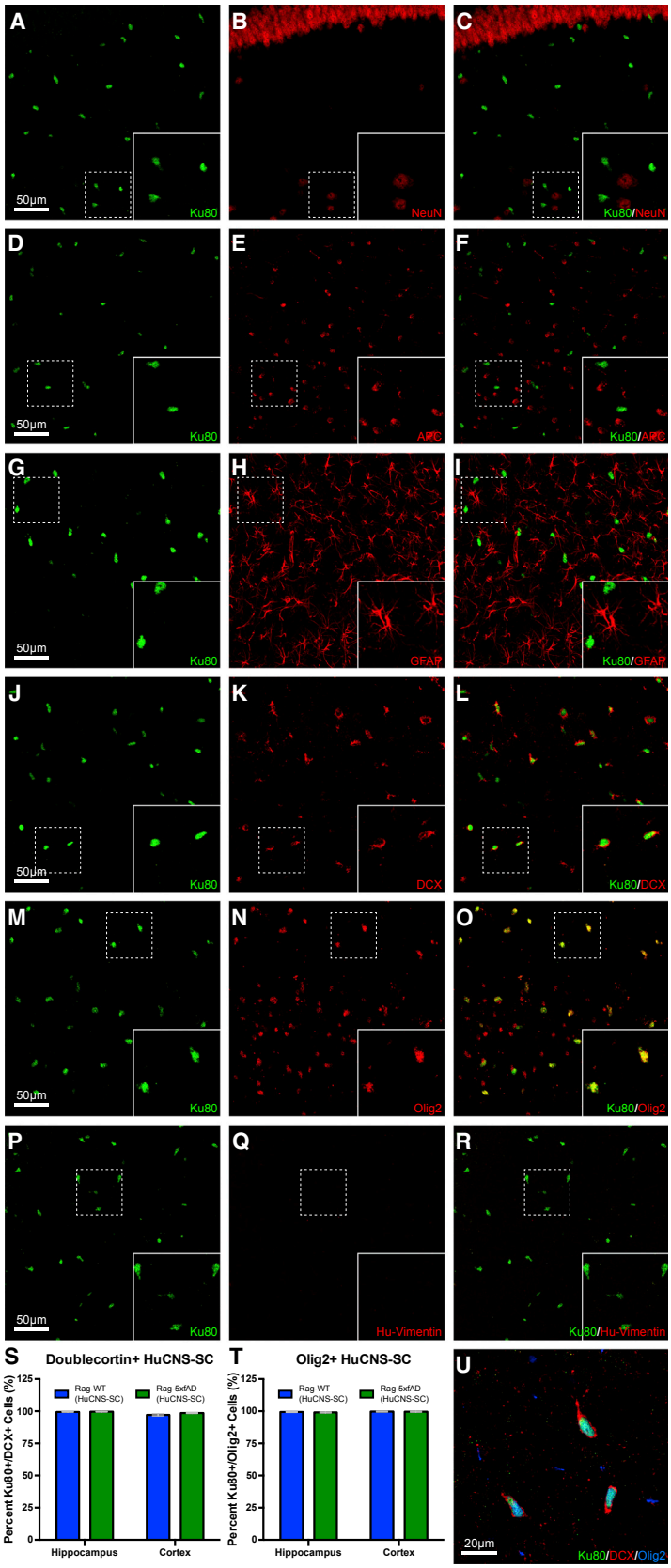

Figure 2. Five Months Post-Transplantation HuCNS-SCs Show No Evidence of Terminal Neuronal or Glial Differentiation

Sections from all animals, both Rag-5xfAD (shown) and Rag-WT, probed with human-specific nuclei marker (Ku80, green) to identify engrafted HuCNS-SCs and co-labeled with mature (A–I) and immature (J–R) markers of neurons, oligodendrocytes, and astrocytes. Co-labeling of HuCNS-SCs with mature neuronal marker NeuN (A–C), mature oligodendroglial marker APC (D–F), and mature astrocytic marker GFAP (G–I) revealed no expression of any mature markers in HuCNS-SCs. Co-labeling of HuCNS-SCs with immature neuronal marker doublecortin (J–L, U) revealed that greater than 97% of engrafted HuCNS-SCs expressed DCX (S). Intriguingly, co-labeling of HuCNS-SCs with immature oligodendrocyte marker Olig2 (M–O, U) revealed that greater than 99% of engrafted HuCNS-SCs also expressed Olig2 (T). However, none of the engrafted HuCNS-SCs expressed immature astrocytic marker vimentin (P–R). Thus, taken together, it appears that HuCNS-SCs fail to terminally differentiate in immune-deficient mouse brains. Data presented as means ± SEM. Two-way ANOVA $p < 0.05$ and Fisher's PLSD post hoc. $N \geq 6$ animals/group and one section/region of interest was analyzed for differentiation. The total number of cells counted was equivalent between genotypes.

Scale bar, 50 μm.

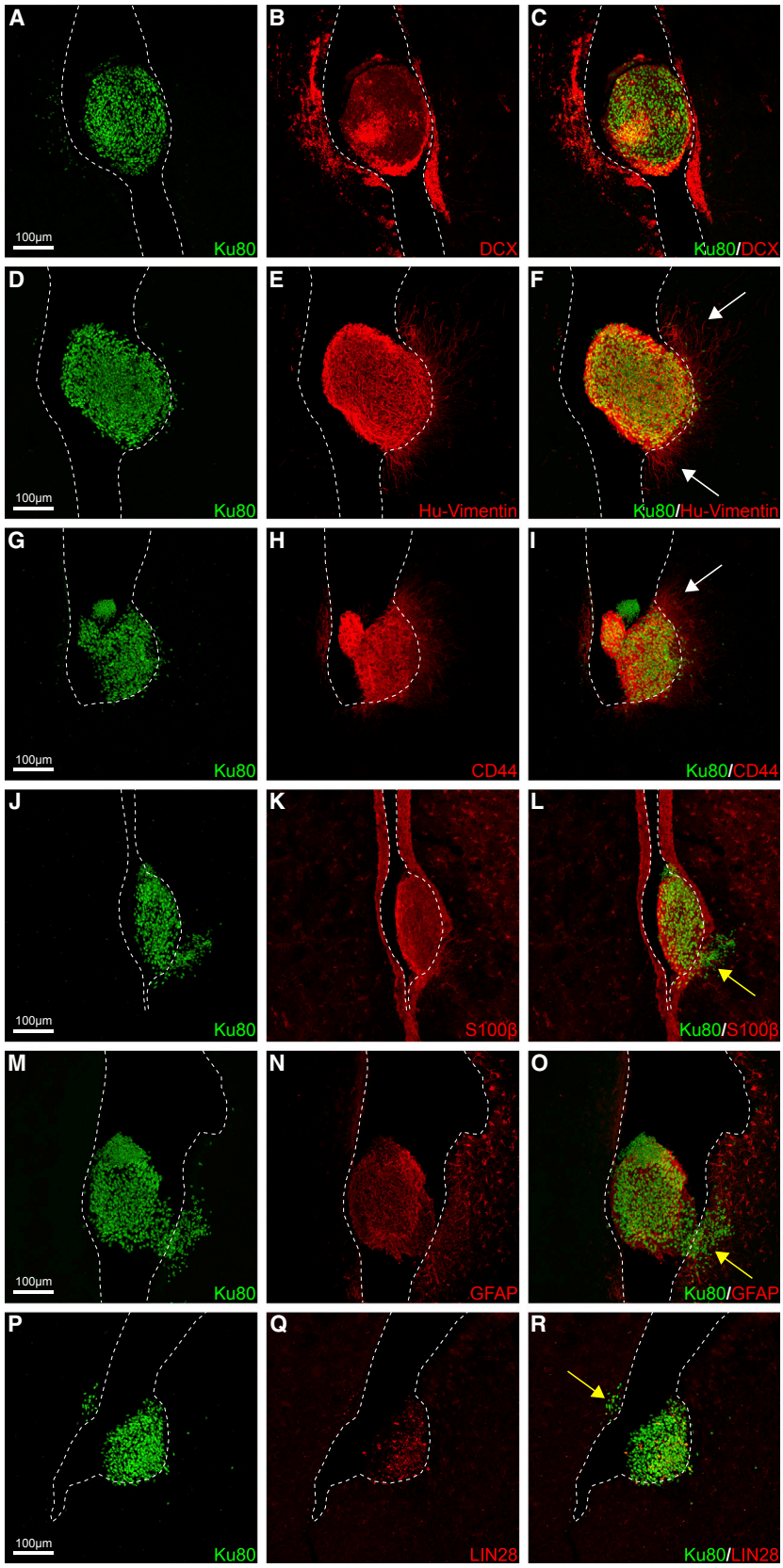

Figure 3. HuCNS-SCs Form Ectopic Clusters within the Lateral Ventricle

Over a quarter of animals that received HuCNS-SCs exhibited ectopic clusters within the anterior lateral ventricle (~+1.5 mm relative to bregma, 3.5 mm from site of injection, +1.5 mm from furthest anterior parenchymal cell migration). Interestingly, HuCNS-SCs within the ventricle were immunoreactive for several immature glial markers that failed to label intraparenchymally engrafted cells. Instead, these HuCNS-SC ventricular clusters (Ku80, green) were immunoreactive for (A–C) DCX (immature neurons, red), (D–F) vimentin (immature glia/neurons, red), (G–I) CD44 (immature glia, red), (J–L) S100β (glia, red), and (M–O) GFAP (astrocytes, red). In some clusters (G and M), examples of what appears to be varying Ku80+ nuclei size or pleomorphism can also be observed. (P–R) Some cells within the ventricles as well infiltrating HuCNS-SCs (arrow in R) were also positive for LIN28, a marker of one type of PNET that exhibits similar characteristic uneven immunoreactivity (Picard et al., 2012). Ventricular clusters also exhibit growth into the surrounding tissue of both fibers (white arrows) and infiltration of cells through the ventricle wall into the adjacent striatum or septum (yellow arrows, see also Movie S2). Dotted lines indicate boundary of ventricle walls.

Scale bar, 100 μm. See also Figures S1 and S2 and Movie S2.

nodular growth pattern, relatively monomorphic and immature appearance, and immature immunophenotype distinct from intraparenchymal cells warrant concern and long-term monitoring even in the absence of overt oncogenesis (see Discussion).

HuCNS-SC Failed to Improve Cognition in Rag-5xfAD Mice

The primary goal of this study was to determine whether HuCNS-SCs could provide long-term benefits to cognitive function. Mice were therefore subjected to a battery of behavioral assessments beginning 4 months post-transplantation. Analysis of the Morris water maze, a well-established task used to assess impairments in hippocampal-dependent learning and memory, found that vehicle-injected and HuCNS-SC-injected Rag-WT mice performed equally well on this task (Figure 4A). Throughout training, Rag-5xfAD vehicle-injected mice (green squares) exhibited typical AD-associated impairments in latency to reach the hidden platform. Transplantation of HuCNS-SCs failed to improve the performance of Rag-5xfAD mice (green triangles) as this group performed equivalent to vehicle-injected Rag-5xfAD mice and significantly worse than both Rag-WT groups (Figure 4A; ANOVA and Fisher's protected least significant difference [PLSD], $p < 0.05$). Probe trial analysis revealed no significant differences between any of the groups (Figure 4A).

Mice were also tested in the novel arm Y maze to measure working memory. Rag-WT (Vehicle) exhibited a significant preference for the novel arm during testing while Rag-5xfAD (Vehicle) had no such preference, confirming a significant impairment in working memory (Figure 4B). HuCNS-SC-treated mice displayed an almost identical phenotype to their vehicle-treated counterparts (Figure 4B), demonstrating again a failure of HuCNS-SC transplantation to rescue AD-associated cognitive deficits.

Analysis of anxiety, using the elevated plus maze, found that both vehicle-injected Rag-WT and Rag-5xfAD mice spent a similar amount of time in the open arm, suggesting that Rag-5xfAD mice do not exhibit any obvious anxiety deficits at this age (Figure 4C). Curiously, a significant difference was observed in anxiety between HuCNS-SC-treated Rag-WT and Rag-5xfAD animals (Figure 4C); the Rag-5xfAD (HuCNS-SC) mice displayed an abnormal reduction in anxiety.

HuCNS-SC Had No Impact on Amyloid Pathology or BDNF

To determine whether HuCNS-SC transplantation modified Aβ pathology, we utilized a highly sensitive multiplex ELISA and found, in agreement with previous studies, that NSC transplantation had no effect on Aβ40 or Aβ42 levels (Figures 4D and 4E; Ager et al., 2015). Furthermore, ELISA measurement of total hippocampal BDNF also showed no significant differences between HuCNS-SC- and vehicle-treated Rag-5xfAD mice (Figure 4F), in contrast to prior studies of murine NSC transplantation in which increased BDNF was critical for cognitive improvements (Blurton-Jones et al., 2009; Goldberg et al., 2015). These data therefore suggest that the lack of cognitive benefit following HuCNS-SC transplantation may be related at least in part to the inability of HuCNS-SC to increase brain BDNF levels.

HuCNS-SC Transplantation Fails to Increase Hippocampal Synaptic Density

Synaptic loss is one of the best correlates with cognitive dysfunction in AD (Terry et al., 1991), and short-term transplantation of either mNSCs or research-grade HuCNS-SCs has previously been shown to increase hippocampal synaptic density in AD mice (Blurton-Jones et al., 2009; Ager et al., 2015). The effect of HuCNS-SCs on hippocampal synapses was therefore examined by quantifying PSD95 levels within the stratum oriens of CA1 via high-magnification confocal z stack images and IMARIS image analysis software (Figures 4G–4J). We found that Rag-5xfAD vehicle-treated animals exhibited a significant decrease in the number of PSD95 puncta compared with Rag-WT vehicle-treated animals (Figure 4K). However, we found that HuCNS-SC transplantation in Rag-5xfAD mice had no beneficial effect on this AD-associated loss in synaptic puncta. On the contrary, we found instead that HuCNS-SC transplantation significantly decreased synaptic density when compared with vehicle-injected Rag-5xfAD mice (Figure 4K). These results demonstrate a lack of synaptic benefit, which correlates with our other results that HuCNS-SCs also failed to increase BDNF or rescue cognitive deficits.

DISCUSSION

Here we report that StemCells, Inc.'s fetal-derived HuCNS-SCs failed to terminally differentiate after long-term transplantation into the brains of immune-deficient WT and AD transgenic mice. We also found that these cells formed ectopic clusters within the lateral ventricles of over a quarter of transplanted animals and had no beneficial effects on cognitive function, BDNF expression, or synaptic density. Our data therefore lead us to conclude that HuCNS-SCs cannot be readily developed toward a clinical application for AD.

These results are in contrast to our previous study that investigated a different research-grade HuCNS-SC line using a short-term transplantation paradigm. Unfortunately, we no longer have access to StemCells, Inc.'s proprietary HuCNS-SC lines and therefore it is difficult to directly

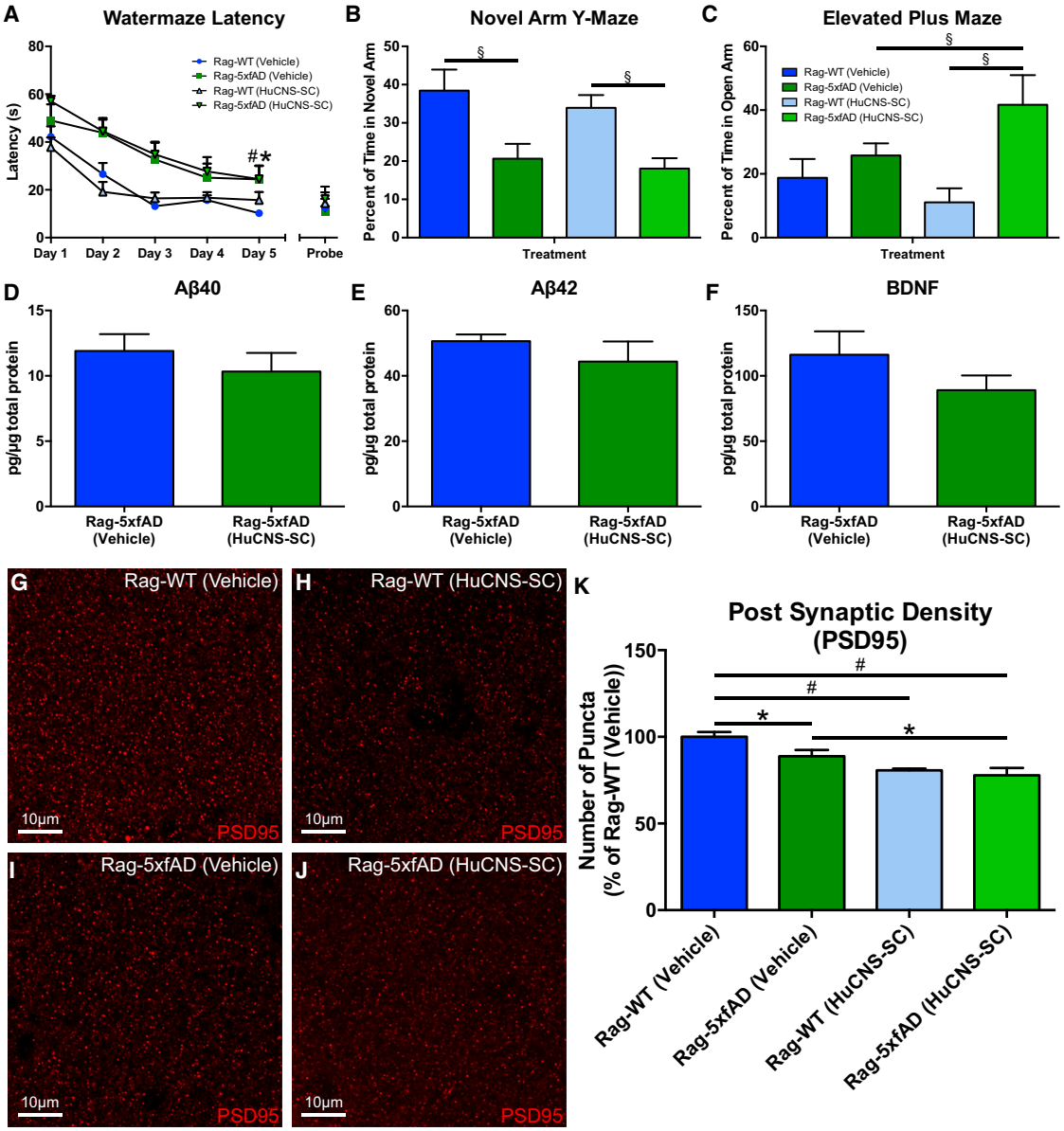

Figure 4. HuCNS-SCs Fail to Improve Learning and Memory in Rag-5xfAD Mice

(A) Analysis of Morris water maze (MWM) learning curve demonstrates that vehicle-injected Rag-5xfAD mice (green squares) take significantly longer to find the platform compared with vehicle-injected Rag-WT mice (blue circles). Thus, Rag-5xfAD mice exhibit characteristic AD-associated impairments in MWM performance. Transplantation of HuCNS-SCs provides no improvement in MWM performance as HuCNS-SC-injected Rag-5xfAD mice (green triangles) perform no better than vehicle-injected Rag-5xfAD mice (green squares).

(B) Rag-5xfAD mice regardless of treatment were also significantly impaired in a novel arm Y-maze test of spatial working memory, spending a smaller percentage of their time in the novel arm.

(C) Analysis of anxiety in elevated plus maze (EPM) revealed no differences between Rag-5xfAD and Rag-WT animals receiving vehicle injections. However, Rag-5xfAD (HuCNS-SC) animals were significantly less anxious than Rag-WT (HuCNS-SC) animals, suggesting that HuCNS-SCs may promote impaired EPM performance.

(D and E) ELISA analysis of hippocampal lysates revealed no difference in Aβ40 or Aβ42 levels regardless of treatment in Rag-5xfAD mice.

(F) HuCNS-SC transplantation also failed to elevate hippocampal BDNF protein levels and surprisingly produced a non-significant trend toward decreased BDNF ($p = 0.21$).

(G–J) Representative high-power confocal images of presynaptic PSD-95 labeling in the stratum oriens of the hippocampus.

(K) As previously reported in AD mouse models, quantification of PSD-95 density revealed a significant reduction in postsynaptic terminals in vehicle-treated Rag-5xfAD versus vehicle-treated Rag-WT mice. However, no increase in PSD95 density was detected after HuCNS-SC

(legend continued on next page)

compare these two sets of results. Rather, we can only speculate as to why the current studies utilizing HuCNS-SCs originally produced under GMP conditions show no efficacy. These HuCNS-SCs differed from those previously utilized in that they were initially derived and passaged under GMP conditions. Although the initial design of this study aimed to test more clinically relevant HuCNS-SCs, when such cells were initially shipped to our laboratory, they exhibited extremely poor viability (<60%) and were not used. To complete the study, HuCNS-SCs were subsequently expanded under non-GMP conditions to the same passage number as the originally planned GMP-grade cells. Therefore, a significant difference between the cells used in this study and those utilized in all previous studies was their initial derivation in the GMP facility. The contrasting results compared with our previous studies with research-grade HuCNS-SCs, and the similar findings reported in the accompanying report by Anderson et al. (2017) highlight the need to stringently test each clinical-grade candidate stem cell line using appropriate long-term in vivo models. While disappointing, our results nevertheless provide important insight into the testing and potential development of stem cell-based therapies for AD.

Although previous studies have demonstrated the ability of research-grade HuCNS-SC lines to differentiate in both immune-suppressed and immune-deficient models (Cummings et al., 2005; Sontag et al., 2014; Ager et al., 2015), we observed no terminal differentiation in the current study. In our prior 1-month study, we reported that research-grade HuCNS-SCs expressed DCX and Olig2 and concluded that these markers demonstrated evidence of early neural and glial differentiation as terminal differentiation would not be expected at this early time point (Ager et al., 2015). However, in the current study, after 5 months we still observed no evidence of terminal differentiation, again detecting expression of only DCX and Olig2 within intraparenchymally engrafted cells. Whereas co-expression of these two markers was not examined in our prior study, triple labeling and quantification in the current report demonstrate that virtually all intraparenchymally localized human cells co-express DCX and Olig2.

One possible explanation for the lack of terminal differentiation is that an intact inflammatory response may be necessary for hNSC differentiation in rodent models. However, previous studies have demonstrated terminal tri-lineage differentiation of a research-grade HuCNS-SC line in an immune-deficient murine spinal cord injury model (Cummings et al., 2005). However, transplantation of HuCNS-SCs into an uninjured spinal cord led to a decrease in mature differentiation (Sontag et al., 2014). Therefore, it remains possible that a specific type of inflammatory response is required to cue NSC differentiation. However, the Rag-5xfAD mice, similar to other transgenic models of AD, exhibit significant innate immune inflammation (Marsh et al., 2016), and yet we observed identical differentiation compared with Rag-WT mice.

In addition to the lack of terminal differentiation, we found that transplantation of HuCNS-SCs led to ectopic ventricular clusters of human cells in 5 of 18 animals. While these findings are concerning, it is important to point out that prior studies have found that other lines of HuCNS-SCs appear safe and do not form tumors following transplantation into immunosuppressed or immune-deficient animal models or in two small phase I trials (Cummings et al., 2005; Tamaki et al., 2009; Gupta et al., 2012; Selden et al., 2013). What then are these cell clusters and why have they not previously been reported? One possibility is that these clusters are formed only by this particular HuCNS-SC line. However, in a small pilot study, we found that a second HuCNS-SC line produced an identical ventricular cluster, suggesting that this may not be the case. Another possibility is that animal studies have previously focused on shorter time points, and clusters have not had sufficient time to form. This is certainly the case for our prior examination of HuCNS-SC transplantation in the 3xTg-AD model that examined only a 1-month time point and detected no such clusters (Ager et al., 2015). It is also possible that ventricular clusters could result from inaccurate stereotactic targeting. However, we verified appropriate targeting of the hippocampus in all animals and confirmed that there was no entry of the needle into the ventricles.

Interestingly, these HuCNS-SC clusters expressed many immature markers of both neurons and astrocytes that are not typically co-expressed in CNS cells and are completely different from the markers expressed by intraparenchymally engrafted hNSCs (Figures 3 and S2J–S2M). These clusters also expressed LIN28, a marker associated with embryonic stem cells that can be found in some NSC lines, where it has been shown to play a role in

transplantation. Instead, delivery of HuCNS-SCs led to a significant further reduction of PSD95 in Rag5xfAD mice and reduced postsynaptic puncta in Rag-WT mice. ANOVA $p < 0.05$ and Fisher's PLSD post hoc *$p < 0.05$, #$p < 0.001$. Aβ and BDNF; PSD95 $N \geq 6$ animals/group. Data presented as means ± SEM. ANOVA $p < 0.05$ and Fisher's PLSD post hoc. $N \geq 6$ animals/group (B–C), $N \geq 4$ animals/group (D–F), (K) $N \geq 6$ animals/group. Value for each animal was an average of five randomly selected regions of interest within images of the stratum oriens of two different brain sections (total of ten measurements). (A) *$p < 0.05$ between Rag-WT (Vehicle) and Rag-5xfAD (Vehicle) and #$p < 0.05$ between Rag-WT (Vehicle) and Rag-5xfAD (HuCNS-SC). (B, C, and K) *$p < 0.05$, §$p < 0.01$, #$p < 0.001$.
Scale bar, 10 μm.

proliferation and differentiation (Darr and Benvenisty, 2009; Kawahara et al., 2011; Cimadamore et al., 2013). LIN28 has also previously been used as a marker of certain CNS neoplasms including PNETs and neurocytomas, which some have hypothesized arise from abnormal NSCs (von Deimling et al., 1990; Hassoun et al., 1993; Hemmati et al., 2003; Singh et al., 2003; Sim et al., 2006; Picard et al., 2012; Rodini et al., 2012).

Given these findings, StemCells, Inc. sponsored a third-party review by a CRO. In this report, the CRO veterinary pathologist concluded that "there is no morphologic evidence of neoplastic transformation in the cell population." The veterinary pathologist also stated that "the cellular morphology is very uniform and no cellular atypia, pleomorphism, mitoses or invasion of the neuroparenchyma is present in any section." An additional review by a practicing board-certified human neuropathologist (E.S.M) largely concurred with the CRO report but also noted that the immunophenotypic features of the cells in the ventricular masses, as seen by both pathologists, were reminiscent of central neurocytoma, a low-grade CNS tumor that often displays neuronal and glial differentiation and is typically intraventricular and thought to arise from abnormal growth of neural progenitors (von Deimling et al., 1990; Hassoun et al., 1993; Sim et al., 2006). The resemblance to central neurocytoma and the differences compared with the intraparenchymally engrafted cells suggest that the extrinsic (cell-cell and intraventricular environments) rather than intrinsic influences drive the neurocytoma-like phenotype. Since the cell clusters were significant distances from confirmed injection sites and from the most rostral intraparenchymally engrafted cells, intraventricular transit of injected HuCNS-SCs is the most likely explanation for their location. Furthermore, the low Ki67 index observed in the intraventricular masses is consistent with the majority of neurocytomas in patients (Hassoun et al., 1993; Söylemezoglu et al., 1997). Optimistically, central neurocytomas are often benign, although one review of more than 70 patients with reported case histories found that patients exhibited intracranial pressure causing papilledema, headaches (which were sometimes the only symptoms), nausea, and vomiting (Hassoun et al., 1993). All of these would be concerns should these HuCNS-SC masses form in human patients and would be difficult to detect in mouse studies when not looking for those types of symptoms beforehand. The CRO pathology report did state that there was no evidence of abnormal cerebrospinal fluid drainage such as hydrocephalus, and we did not note any abnormal clinical signs during behavioral testing or post hoc pathological analysis.

The consistent low-grade features of the intraventricular clusters noted by both pathologists may reflect a "normal" HuCNS-SC phenotype rather than an abnormal oncogenic phenotype per se, although this cannot be rigorously determined from our study alone and does not necessarily indicate there are no safety concerns. When put in context with the lack of terminal differentiation displayed by the intraparenchymal cells and the lack of similar clusters reported in the NSC engraftment literature, our findings raise the possibility of an intrinsic predisposition to a neurocytoma-like growth pattern. Moreover, their appearance in multiple animals, significant distance from injection sites and intraparenchymally engrafted cells, nodular intraventricular growth pattern, and monomorphic immature phenotype distinct from the intraparenchymal cells would clearly warrant great caution and long-term patient monitoring even in the absence of overt oncogenic or high-grade features. Furthermore, some of the clusters observed appeared to have broken through the ventricle wall and begun to invade the adjacent striatal tissue (Figures 3L, 3O, and 3R, yellow arrows; Movie S2), suggesting they could potentially influence the circuitry or function of unintended brain regions such as the striatum. Importantly, however, human data collected at 2 years postsurgery and 1 year after cessation of immune suppression indicate that transplantation of 200 million HuCNS-SCs directly into the lateral ventricles is safe, and magnetic resonance imaging and histopathological analysis failed to detect the presence of any abnormal ventricular engraftment or reaction (Selden et al., 2013). Unfortunately, without further access to HuCNS-SCs, there are several questions on which we can only speculate. While not observed in previous patient studies, we were unable to examine whether HuCNS-SCs injected directly into the ventricles followed similar growth patterns to the clusters observed in the current study. Furthermore, we are unsure exactly how HuCNS-SCs entered the ventricles of these animals. During our analysis, we verified the hippocampal targeting of the injection and saw no evidence of ventricular entry by the needle. Among the most rostrally located HuCNS-SCs were cells in the fornix adjacent to the ventricles, and it is possible that a few cells may have crossed the ependymal layer and reached the ventricle in this area. Once there, the HuCNS-SCs would be exposed to many of the same signals that promote endogenous ventricular neurogenesis, allowing them to proliferate. These results and the questions raised, as well as a recent case report (Berkowitz et al., 2016) describing a glioproliferative lesion following spinal cord NSC transplantation by an unregulated clinic, further highlight the critical need to carefully regulate NSC research and to test individual lines in long-term preclinical models prior to clinical translation.

While the lack of terminal differentiation and ectopic ventricular clusters became a major focus of our investigation, we were similarly surprised by the lack of cognitive improvement following HuCNS-SC transplantation. We

have previously found that NSC-derived BDNF can play a critical role in stem cell-mediated improvements in cognition and synaptogenesis (Blurton-Jones et al., 2009). Thus, the lack of BDNF induction by HuCNS-SCs (Figure 4F) may explain the corresponding lack of cognitive and synaptic effects. While the dose of transplanted cells could also influence this, we transplanted an identical number of cells in prior effective studies of murine and hNSC transplantation; thus, we speculate that the specific cell line used may be more important. In support of this, the accompanying report (Anderson et al., 2017) performed a direct comparison between research-grade and "clinically intended cell line" HuCNS-SCs that further demonstrates that significant inherent differences exist between individual HuCNS-SC lines derived from different donors or initially produced in research versus GMP settings.

Another potential explanation for the lack of behavioral and synaptic efficacy in the current study is the severity of Aβ pathology that occurs in the 5xfAD transgenic model. These mice develop extensive plaque pathology at a much younger age and faster rate than 3xTg-AD mice, which were used in our prior short-term studies. However, several reports have demonstrated the ability of a variety of different therapeutics, including compounds that increase BDNF, to rescue both synaptic loss and cognitive deficits in the 5xfAD model (Hongpaisan et al., 2011; Devi and Ohno, 2012; Spangenberg et al., 2016). Although the results of the accompanying study by Anderson et al. (2017) lead us to conclude that the differences between research-grade and HuCNS-SCs initially derived under GMP conditions are the more likely culprit, we cannot completely preclude that the magnitude of plaque pathology or alternatively the lack of tau pathology in this specific model differentially influences NSC efficacy in comparison with other AD models such as 3xTg-AD mice.

In conclusion, while the primary results of this study are negative, there are several valuable lessons that can be learned from our findings. Chief among them is the need to stringently test the long-term efficacy and safety of hNSCs in appropriate animal models and to prescreen candidate NSC lines for factors or other attributes such as BDNF that have been implicated in efficacy. Use of high-throughput genomic analysis will likely also be critically important to identify any concerning genetic differences between lines from different donor material or identify mutations or SNPs that could influence safety or efficacy. The contrasting results of this study compared with our previously published data, as well as the accompanying report by Anderson et al. (2017) directly comparing two different HuCNS-SC lines in a model of spinal cord injury, emphasize the need to directly examine each newly derived cell line compared with previous lines even if the lines were derived and cultured under equivalent or even identical fashion. This is especially critical for NSC therapies that are derived from varying fetal tissue sources but also appears to apply for embryonic stem cells and induced pluripotent stem cells derived from different subjects. It also stresses the need to test therapeutics in a variety of animal models and analyze results of multiple studies as different preclinical models offer varying advantages and disadvantages. We also would like to propose that this study serve as an example of the importance of publishing negative results from preclinical studies. Publication bias has no doubt led to significant problems with our understanding of stem cell therapies and the risks and difficulties associated with them. Not only are these data informative but we would argue that understanding and examining negative data such as these is essential for the eventual development of safe and effective stem cell therapies.

EXPERIMENTAL PROCEDURES

HuCNS-SCs

Two HuCNS-SC lines were generously provided by StemCells, Inc. All derivation, maintenance, passaging, and preparation for shipment were performed by StemCells, Inc. HuCNS-SCs are derived via fluorescence-activated cell sorting from donated fetal brain tissue for the stem cell marker CD133+, a lack of the hematopoietic markers CD34− and CD45−, and low levels of $CD24^{lo}$ (Uchida et al., 2000). Cells were initially produced, maintained, and passaged by StemCells, Inc. under GMP conditions. A vial of frozen P3 GMP cells was transferred to the PD laboratory, which then generated a bank of P6 cells. The first batch of cells for the current study was generated in the PD laboratory, resulting in P10 cells that, upon shipment to the University of California–Irvine, exhibited poor viability (~60%) and were therefore not used. Instead, additional frozen vials of P6 cells were transferred from the PD to StemCells, Inc.'s research laboratory and expanded for four additional passages before overnight shipment. These cells were then centrifuged, washed, and counted immediately prior to transplantation. Each day of surgery was performed with a new shipment of cells and viability of cells reported by StemCells, Inc. prior to shipment was 94% and 92% on days 1 and 2, respectively. The cells used in the current study were expanded from P3 to P10 outside of the GMP facility using non-GMP reagents and protocols and therefore are not GMP grade. Details regarding the stereotactic transplantation of HuCNS-SCs are provided in the Supplemental Experimental Procedures.

Cognitive Testing

All animal procedures were performed in strict accordance with the National Institutes of Health and University of California Institutional Animal Care and Use Committee.

At 6 months of age (4 months post-transplantation), mice were subjected to a battery of behavioral and cognitive tasks. All animals were habituated to handling prior to the beginning of behavioral testing. All behavioral testing was performed in random order by an experimenter blinded to animal genotype and treatment. Cognition was examined using the Morris water maze and novel

arm Y-maze tasks, and anxiety was examined using the elevated plus maze task (Supplemental Experimental Procedures). All behavioral tasks were recorded on video, and analysis was performed by an observer blinded to genotype and treatment using unbiased analysis software ANY-Maze (Stoelting) or Noldus Ethovision (Noldus).

Immunohistochemistry and Biochemistry

Following completion of all behavioral testing, mice were anesthetized with Euthasol prior to intracardial perfusion with 0.01 M PBS. Brains were removed and processed for biochemical and immunohistological analyses as detailed in the Supplemental Experimental Procedures.

Statistical Analysis

Statistical analysis was performed using GraphPad Prism statistics software. Comparisons involving more than two groups utilized one-way ANOVA followed by Fisher's post hoc test. Comparisons of two groups utilized two-tailed Students t test. Differences were considered significant when $p < 0.05$ for both ANOVA and post hoc tests.

SUPPLEMENTAL INFORMATION

Supplemental Information includes Supplemental Experimental Procedures, two figures, and two movies and can be found with this article online at http://dx.doi.org/10.1016/j.stemcr.2016.12.019.

AUTHOR CONTRIBUTIONS

S.E.M. and M.B.-J. designed the research; S.E.M., S.T.Y, M.T., L.L., J.L.D., W.W.P., and M.B.-J. performed the research; S.E.M., S.T.Y., M.T., E.S.M., W.W.P., and M.B.-J. analyzed data; and S.E.M and M.B.-J. wrote the paper.

ACKNOWLEDGMENTS

This work was supported in part by NIH RF1AG048099 (M.B.-J.), NIH P50 AG016573 (W.W.P. and M.B.-J.), gs2:Alzheimer's Association BFG-14-317000 (M.B.-J.), departmental start-up funds (M.B.-J), NIA T32 AG00096-30 (S.E.M.), NINDS T32 NS082174-01 (S.E.M.), and NIH Shared Instrumentation OD010420. Special thanks to Dr. David Baglietto-Vargas for assistance and training in stereology. HuCNS-SCs and injection buffer were generously provided by StemCells, Inc.

Received: June 30, 2016
Revised: October 28, 2016
Accepted: December 19, 2016
Published: February 14, 2017

REFERENCES

Ager, R.R., Davis, J.L., Agazaryan, A., Benavente, F., Poon, W.W., LaFerla, F.M., and Blurton-Jones, M. (2015). Human neural stem cells improve cognition and promote synaptic growth in two complementary transgenic models of Alzheimer's disease and neuronal loss. Hippocampus *25*, 813–826.

Alzheimer's Association. (2016). 2016 Alzheimer's disease facts and figures. Alzheimers Dement *12*, 459–509.

Anderson, A.J., Haus, D.L., Hooshmand, M.J., Perez, H., Sontag, C.J., and Cummings, B.J. (2011). Achieving stable human stem cell engraftment and survival in the CNS: is the future of regenerative medicine immunodeficient. Regen. Med. *6*, 367–406.

Anderson, A.J., Piltti, P.M., Hooshmand, M.J., Nishi, R.A., and Cummings, B.J. (2017). Preclinical Efficacy Failure of Human CNS-Derived Stem Cells for Use in the Pathway Study of Cervical Spinal Cord Injury. Stem Cell Rep. *8*, in this issue.

Berkowitz, A.L., Miller, M.B., Mir, S.A., Cagney, D., Chavakula, V., Guleria, I., Aizer, A., Ligon, K.L., and Chi, J.H. (2016). Glioproliferative lesion of the spinal cord as a complication of "Stem-Cell Tourism". N. Engl. J. Med. *375*, 196–198.

Blurton-Jones, M., Kitazawa, M., Martinez-Coria, H., Castello, N.A., Muller, F.J., Loring, J.F., Yamasaki, T.R., Poon, W.W., Green, K.N., and LaFerla, F.M. (2009). Neural stem cells improve cognition via BDNF in a transgenic model of Alzheimer disease. Proc. Natl. Acad. Sci. USA *106*, 13594–13599.

Blurton-Jones, M., Spencer, B., Michel, S., Castello, N.A., Agazaryan, A.A., Davis, J.L., Müller, F.-J., Loring, J.F., Masliah, E., and LaFerla, F.M. (2014). Neural stem cells genetically-modified to express neprilysin reduce pathology in Alzheimer transgenic models. Stem Cells Res. Ther. *5*, 46.

Cimadamore, F., Amador-Arjona, A., Chen, C., Huang, C.T., and Terskikh, A.V. (2013). SOX2-LIN28/let-7 pathway regulates proliferation and neurogenesis in neural precursors. Proc. Natl. Acad. Sci. USA *110*, E3017–E3026.

Cummings, B.J., Uchida, N., Tamaki, S.J., Salazar, D.L., Hooshmand, M., Summers, R., Gage, F.H., and Anderson, A.J. (2005). Human neural stem cells differentiate and promote locomotor recovery in spinal cord-injured mice. Proc. Natl. Acad. Sci. USA *102*, 14069–14074.

Darr, H., and Benvenisty, N. (2009). Genetic analysis of the role of the reprogramming gene LIN-28 in human embryonic stem cells. Stem Cells *27*, 352–362.

Devi, L., and Ohno, M. (2012). 7,8-dihydroxyflavone, a small-molecule TrkB agonist, reverses memory deficits and BACE1 elevation in a mouse model of Alzheimer's disease. Neuropsychopharmacology *37*, 434–444.

Ebert, A.D., Beres, A.J., Barber, A.E., and Svendsen, C.N. (2008). Human neural progenitor cells over-expressing IGF-1 protect dopamine neurons and restore function in a rat model of Parkinson's disease. Exp. Neurol. *209*, 213–223.

Goldberg, N.R., Caesar, J., Park, A., Sedgh, S., Finogenov, G., Masliah, E., Davis, J., and Blurton-Jones, M. (2015). Neural stem cells rescue cognitive and motor dysfunction in a transgenic model of dementia with Lewy bodies through a BDNF-dependent mechanism. Stem Cell Reports *5*, 791–804.

Gupta, N., Henry, R.G., Strober, J., Kang, S.M., Lim, D.A., Bucci, M., Caverzasi, E., Gaetano, L., Mandelli, M.L., Ryan, T., et al. (2012). Neural stem cell engraftment and myelination in the human brain. Sci. Transl. Med. *4*, 155ra137.

Hampton, D.W., Webber, D.J., Bilican, B., Goedert, M., Spillantini, M.G., and Chandran, S. (2010). Cell-mediated neuroprotection

in a mouse model of human tauopathy. J. Neurosci. *30*, 9973–9983.

Hassoun, J., Söylemezoglu, F., Gambarelli, D., Figarella-Branger, D., von Ammon, K., and Kleihues, P. (1993). Central neurocytoma: a synopsis of clinical and histological features. Brain Pathol. *3*, 297–306.

Hemmati, H.D., Nakano, I., Lazareff, J.A., Masterman-Smith, M., Geschwind, D.H., Bronner-Fraser, M., and Kornblum, H.I. (2003). Cancerous stem cells can arise from pediatric brain tumors. Proc. Natl. Acad. Sci. USA *100*, 15178–15183.

Hongpaisan, J., Sun, M.K., and Alkon, D.L. (2011). PKC ε activation prevents synaptic loss, Aβ elevation, and cognitive deficits in Alzheimer's disease transgenic mice. J. Neurosci. *31*, 630–643.

Jiang, P., Chen, C., Wang, R., Chechneva, O.V., Chung, S.H., Rao, M.S., Pleasure, D.E., Liu, Y., Zhang, Q., and Deng, W. (2013). hESC-derived Olig2+ progenitors generate a subtype of astroglia with protective effects against ischaemic brain injury. Nat. Commun. *4*, 2196.

Kawahara, H., Okada, Y., Imai, T., Iwanami, A., Mischel, P.S., and Okano, H. (2011). Musashi1 cooperates in abnormal cell lineage protein 28 (Lin28)-mediated let-7 family microRNA biogenesis in early neural differentiation. J. Biol. Chem. *286*, 16121–16130.

Laywell, E.D., Rakic, P., Kukekov, V.G., Holland, E.C., and Steindler, D.A. (2000). Identification of a multipotent astrocytic stem cell in the immature and adult mouse brain. Proc. Natl. Acad. Sci. USA *97*, 13883–13888.

Marsh, S.E., Abud, E.M., Lakatos, A., Karimzadeh, A., Yeung, S.T., Davtyan, H., Fote, G.M., Lau, L., Weinger, J.G., Lane, T.E., et al. (2016). The adaptive immune system restrains Alzheimer's disease pathogenesis by modulating microglial function. Proc. Natl. Acad. Sci. USA *113*, E1316–E1325.

Mollison, K.W., Fey, T.A., Krause, R.A., Andrews, J.M., Bretheim, P.T., Cusick, P.K., Hsieh, G.C., and Luly, J.R. (1998). Nephrotoxicity studies of the immunosuppressants tacrolimus (FK506) and ascomycin in rat models. Toxicology *125*, 169–181.

Njie, E.G., Kantorovich, S., Astary, G.W., Green, C., Zheng, T., Semple-Rowland, S.L., Steindler, D.A., Sarntinoranont, M., Streit, W.J., and Borchelt, D.R. (2012). A preclinical assessment of neural stem cells as delivery vehicles for anti-amyloid therapeutics. PLoS One *7*, e34097.

Oakley, H., Cole, S.L., Logan, S., Maus, E., Shao, P., Craft, J., Guillozet-Bongaarts, A., Ohno, M., Disterhoft, J., Van Eldik, L., et al. (2006). Intraneuronal beta-amyloid aggregates, neurodegeneration, and neuron loss in transgenic mice with five familial Alzheimer's disease mutations: potential factors in amyloid plaque formation. J. Neurosci. *26*, 10129–10140.

Picard, D., Miller, S., Hawkins, C.E., Bouffet, E., Rogers, H.A., Chan, T.S.Y., Kim, S.-K., Ra, Y.-S., Fangusaro, J., Korshunov, A., et al. (2012). Markers of survival and metastatic potential in childhood CNS primitive neuro-ectodermal brain tumours: an integrative genomic analysis. Lancet Oncol. *13*, 838–848.

Rodini, C.O., Suzuki, D.E., Saba-Silva, N., Cappellano, A., de Souza, J.E., Cavalheiro, S., Toledo, S.R., and Okamoto, O.K. (2012). Expression analysis of stem cell-related genes reveal OCT4 as a predictor of poor clinical outcome in medulloblastoma. J. Neurooncol. *106*, 71–79.

Rozkalne, A., Hyman, B.T., and Spires-Jones, T.L. (2011). Calcineurin inhibition with FK506 ameliorates dendritic spine density deficits in plaque-bearing Alzheimer model mice. Neurobiol. Dis. *41*, 650–654.

Ryu, J.K., Cho, T., Wang, Y.T., and McLarnon, J.G. (2009). Neural progenitor cells attenuate inflammatory reactivity and neuronal loss in an animal model of inflamed AD brain. J. Neuroinflammation *6*, 39.

Schenk, D., Basi, G.S., and Pangalos, M.N. (2012). Treatment strategies targeting amyloid beta-protein. Cold Spring Harb. Perspect. Med. *2*, a006387.

Selden, N.R., Al-Uzri, A., Huhn, S.L., Koch, T.K., Sikora, D.M., Nguyen-Driver, M.D., Guillaume, D.J., Koh, J.L., Gultekin, S.H., Anderson, J.C., et al. (2013). Central nervous system stem cell transplantation for children with neuronal ceroid lipofuscinosis. J. Neurosurg. Pediatr. *11*, 643–652.

Sevigny, J., Chiao, P., Bussière, T., Weinreb, P.H., Williams, L., Maier, M., Dunstan, R., Salloway, S., Chen, T., Ling, Y., et al. (2016). The antibody aducanumab reduces Aβ plaques in Alzheimer's disease. Nature *537*, 50–56.

Sim, F.J., Keyoung, H.M., Goldman, J.E., Kim, D.K., Jung, H.W., Roy, N.S., and Goldman, S.A. (2006). Neurocytoma is a tumor of adult neuronal progenitor cells. J. Neurosci. *26*, 12544–12555.

Singh, S.K., Clarke, I.D., Terasaki, M., Bonn, V.E., Hawkins, C., Squire, J., and Dirks, P.B. (2003). Identification of a cancer stem cell in human brain tumors. Cancer Res. *63*, 5821–5828.

Sontag, C.J., Uchida, N., Cummings, B.J., and Anderson, A.J. (2014). Injury to the spinal cord niche alters the engraftment dynamics of human neural stem cells. Stem Cell Reports *2*, 620–632.

Söylemezoglu, F., Scheithauer, B.W., Esteve, J., and Kleihues, P. (1997). Atypical central neurocytoma. J. Neuropathol. Exp. Neurol. *56*, 551–556.

Spangenberg, E.E., Lee, R.J., Najafi, A.R., Rice, R.A., Elmore, M.R., Blurton-Jones, M., West, B.L., and Green, K.N. (2016). Eliminating microglia in Alzheimer's mice prevents neuronal loss without modulating amyloid-β pathology. Brain *139*, 1265–1281.

Suzuki, M., McHugh, J., Tork, C., Shelley, B., Klein, S.M., Aebischer, P., and Svendsen, C.N. (2007). GDNF secreting human neural progenitor cells protect dying motor neurons, but not their projection to muscle, in a rat model of familial ALS. PLoS One *2*, e689.

Taglialatela, G., Hogan, D., Zhang, W.R., and Dineley, K.T. (2009). Intermediate- and long-term recognition memory deficits in Tg2576 mice are reversed with acute calcineurin inhibition. Behav. Brain Res. *200*, 95–99.

Tamaki, S.J., Jacobs, Y., Dohse, M., Capela, A., Cooper, J.D., Reitsma, M., He, D., Tushinski, R., Belichenko, P.V., Salehi, A., et al. (2009). Neuroprotection of host cells by human central nervous system stem cells in a mouse model of infantile neuronal ceroid lipofuscinosis. Cell Stem Cell *5*, 310–319.

Terry, R.D., Masliah, E., Salmon, D.P., Butters, N., DeTeresa, R., Hill, R., Hansen, L.A., and Katzman, R. (1991). Physical basis of cognitive alterations in Alzheimer's disease: synapse loss is the major correlate of cognitive impairment. Ann. Neurol. *30*, 572–580.

Uchida, N., Buck, D.W., He, D., Reitsma, M.J., Masek, M., Phan, T.V., Tsukamoto, A.S., Gage, F.H., and Weissman, I.L. (2000). Direct

isolation of human central nervous system stem cells. Proc. Natl. Acad. Sci. USA *97*, 14720–14725.

von Deimling, A., Janzer, R., Kleihues, P., and Wiestler, O.D. (1990). Patterns of differentiation in central neurocytoma. An immunohistochemical study of eleven biopsies. Acta Neuropathol. *79*, 473–479.

Wang, J., O'Bara, M.A., Pol, S.U., and Sim, F.J. (2013). CD133/CD140a-based isolation of distinct human multipotent neural progenitor cells and oligodendrocyte progenitor cells. Stem Cells Dev. *22*, 2121–2131.

Yamasaki, T.R., Blurton-Jones, M., Morrissette, D.A., Kitazawa, M., Oddo, S., and LaFerla, F.M. (2007). Neural stem cells improve memory in an inducible mouse model of neuronal loss. J. Neurosci. *27*, 11925–11933.

Zhao, C., Deng, W., and Gage, F.H. (2008). Mechanisms and functional implications of adult neurogenesis. Cell *132*, 645–660.

Stem Cell Reports, Volume *8*

Supplemental Information

HuCNS-SC Human NSCs Fail to Differentiate, Form Ectopic Clusters, and Provide No Cognitive Benefits in a Transgenic Model of Alzheimer's Disease

Samuel E. Marsh, Stephen T. Yeung, Maria Torres, Lydia Lau, Joy L. Davis, Edwin S. Monuki, Wayne W. Poon, and Mathew Blurton-Jones

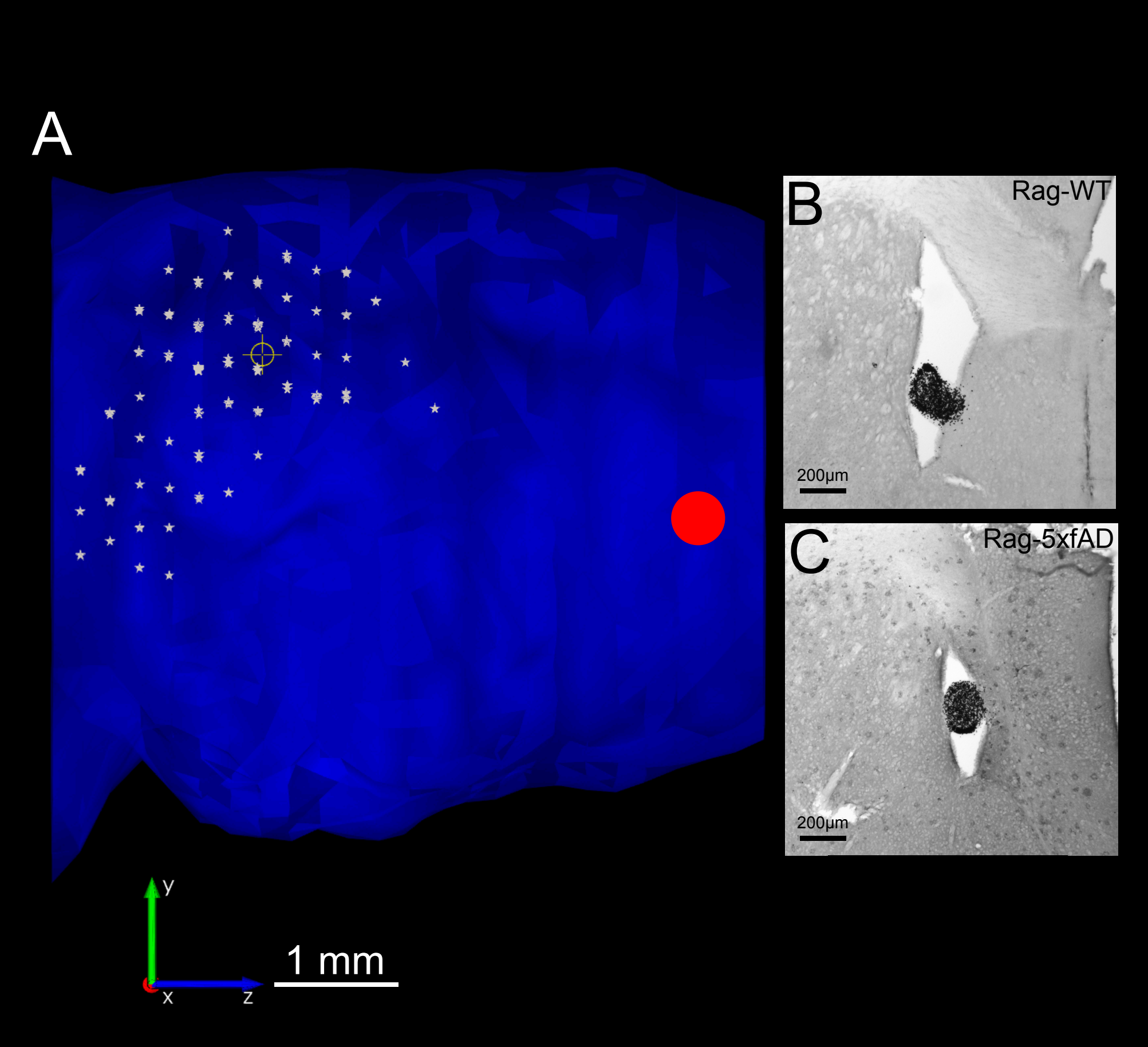
A
B
Rag-WT
200µm
C
Rag-5xfAD
200µm
y
x
z
1 mm

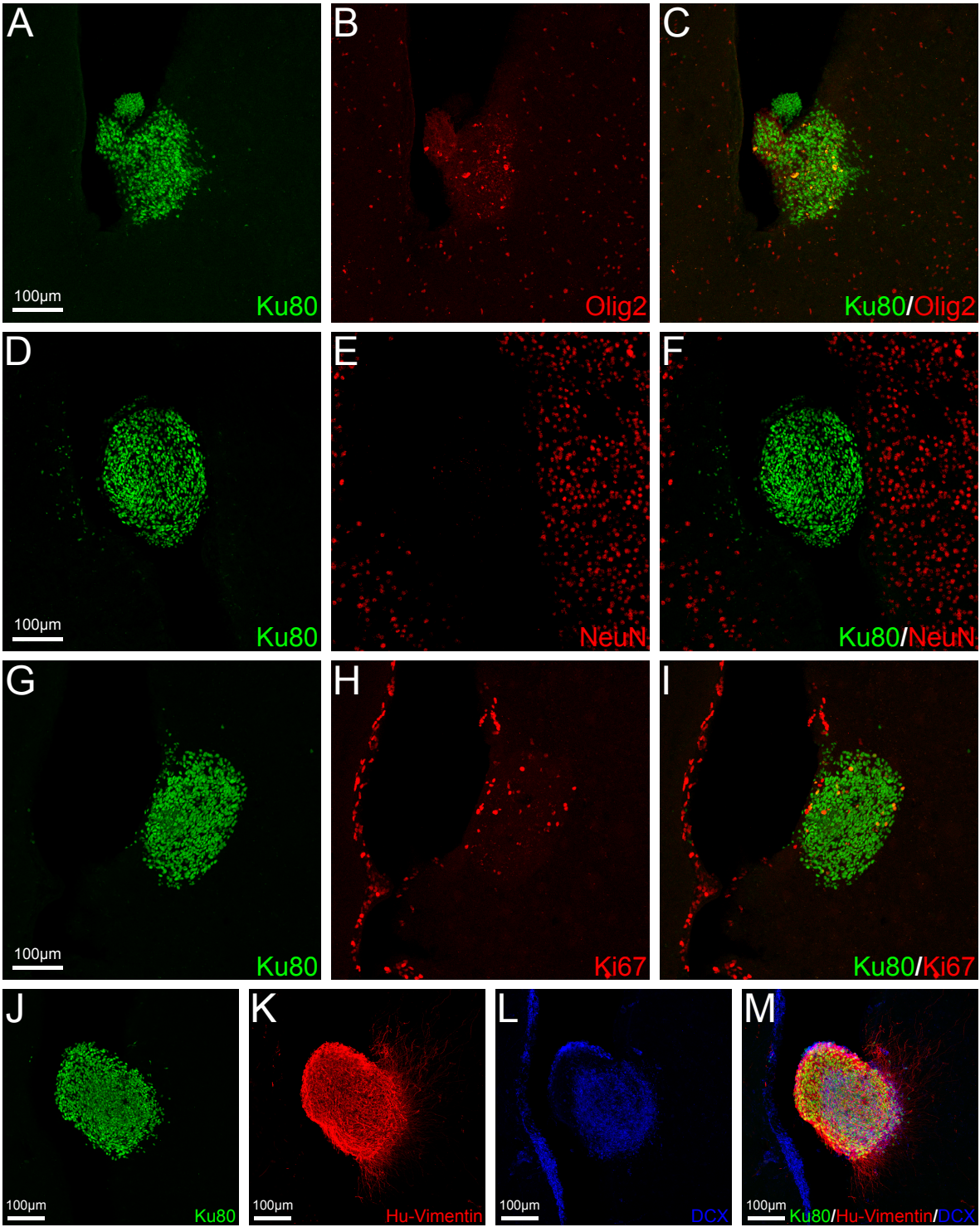
A
100μm
Ku80
B
Olig2
C
Ku80/Olig2
D
100μm
Ku80
E
NeuN
F
Ku80/NeuN
G
100μm
Ku80
H
Ki67
I
Ku80/Ki67
J
100μm
Ku80
K
100μm
Hu-Vimentin
L
100μm
DCX
M
100μm
Ku80/Hu-Vimentin/DCX

Supplemental Figure Legends:

Figure S1: 3D Reconstruction of the location of ventricular cell clusters and intraparenchymal HuCNS-SC engraftment (Related to Figure 3). (A) Side view of Supplemental Movie 1. 3D surface reconstruction of mouse half brain and migration span of HuCNS-SCs based on sections utilized for unbiased stereological analysis. White stars represent individual cells counted in randomly sampled counting frames during unbiased stereological analysis. Yellow bullseye represents location of injection site as verified during stereological analysis. Red sphere represents approximate anterior/posterior localization of ectopic cells clusters found in 5 of 18 animals. **(B-C)** Representative light level immunolabeling of Ku80+ HuCNS-SC within the anterior portion of the lateral ventricle in both Rag-WT **(B)** and Rag-5xfAD **(C)** animals. **(A)** Scale Bar = 1mm, **(B-C)** 200μm.

Figure S2: A small percentage of ventricular-localized HuCNS-SC express Ki67 or Olig2, but not NeuN (Related to Figure 3). (A-C) Unlike engrafted cells within the hippocampus, which are nearly 100% positive for immature oligodendrocyte marker Olig2, only a small number of HuCNS-SC within the ventricles co-label with Olig2. **(D-F)** HuCNS-SC ventricular clusters also do not express the mature neuronal marker NeuN. **(G-I)** Clusters exhibit low levels (3.7%) of Ki67 reactivity. **(J-M)** Representative images demonstrating the co-labeling of glial and neuronal markers within the ventricular clusters. (**J-K)** Are the same images shown in **D-F of Figure 3** demonstrating here the co-expression of the glial marker vimentin and **(L-M)** the neuronal marker doublecortin (DCX). Scale Bar =100μm.

Movie S1: 3D Reconstruction of HuCNS-SC engraftment in a Rag-WT mouse (Related to Figure 1). 3D surface reconstruction of mouse half brain and migration span of HuCNS-SC based on sections utilized for unbiased stereological analysis of HuCNS-SC engraftment. White stars represent individual cells counted in randomly sampled counting frames during unbiased stereological analysis. Yellow bullseye represents location of injection site.

Movie S2: 3D Reconstruction of ventricular HuCNS-SC cells infiltrating the adjacent striatum (Related to Figure 3). 3D surface reconstruction of confocal z stack shown in Panel L of Figure 3. Ku80+ cells (red) can be seen in an ectopic cluster within the lateral ventricle. Ventricular-localized HuCNS-SC cells are positive for S100β and the host ventricle wall also highly expresses S100β, clearly delineating its boundaries. As the image rotates, a clear example of disruption of the ventricle wall (lack of S100β) is accompanied by infiltration of HuCNS-SCs beyond the ventricular boundary and into the surrounding parenchyma.

Supplemental Experimental Procedures:

Mice

Briefly, 5xfAD mice (MMRRC Strain: 034848-JAX), express two co-integrated and co-inherited mutant human transgenes (*APP* and *PSEN1*) under control of the murine Thy1.2 promoter (Oakley et al., 2006; Jawhar et al., 2012; Eimer and Vassar, 2013). Purebred C57Bl6 5xfAD were backcrossed with Rag2/il2rγ double knockout mice (Taconic #4111) (Cao et al., 1995), followed by repeated littermate crosses from each generation, to create mice that are heterozygous for the *APP*/*PSEN1*transgenes and lack both copies of the *RAG2* and *IL2RG* genes. The resulting mice, termed Rag-5xfAD, exhibit characteristic AD plaque pathology, microgliosis, and astrocytosis**,** but lack T-cells, B-cells, and NK-cells that normally mediate xenotransplant rejection (Marsh et al., 2016). Immune-incompetent sex- and age-matched littermate controls hereafter referred to as Rag-WT were also used. Mice were group housed (2-4 mice/cage) on a 12h/12h light/dark cycle with access to food and water *ad libitum*. All animal procedures were performed in strict accordance to the National Institutes of Health and University of California animal care and use guidelines.

Stereotactic HuCNS-SC Transplantation Surgery

Prior to surgeries, cells were counted and assessed for viability and then resuspended in injection buffer (X-VIVO 15 media (Lonza; Basel, Switzerland) with anti-oxidant supplement, generously provided by Stem Cells Inc.) at a concentration of 50,000 cells/µl. Cell viability measured before surgery was 85.9% and 82.6% on days 1 and 2 respectively. Vehicle and cell surgeries were performed on both Rag-5xfAD and Raw mice on both days of surgery. Surgeries were performed on 2 month old mice using hippocampal coordinates AP: -2.06, ML: ± 1.75, DV: - 1.95 relative to Bregma. Accuracy of injection sites was confirmed by subsequent post-mortem visualization of the needle tract in coronal brain sections of all animals. Cells were bilaterally injected using a 10µl Hamilton microsyringe (30-gauge), in volume of 2µl (100,000 cells total/hemisphere; 200,000 cells/animal) at rate of 1 µl/min. Following the injection the syringe remained in place for a period of 4 minutes before being slowly withdrawn to minimize potential reflux of the cells along the needle track. Surgical incisions were closed with Tissuemend (VetEquip) and mice were allowed to recover on a heating pad before being placed back in to their home cage. Following completion of the surgeries, the remaining cells were again counted and assessed for viability for comparison to pre-surgical counts. Cell viability following completion of surgeries (~3.5 hours post-initial count) was 76.3% and 77.3% on days 1 and 2 respectively (5-10% decreased viability).

Morris Water Maze

The task consists of a pool of opaque white water to obscure the location of hidden escape platform submerged just beneath the water's surface. On all walls surrounding the pool were high-contrast, easily visible spatial cues. Mice were placed in pool at randomly assigned starting positions and allowed to swim freely until they reached the platform or 60 seconds elapsed, which ever came first. If the mouse found the platform they were allowed to remain there for 15 seconds before being removed to a pre-warmed holding cage. If the mouse failed to find the platform, they were gently guided by the experimenter to the platform and remained there for 15 seconds before being returning to the warming cage. Mice were given 4 trials per day and placed at different starting positions for each trial. The order of these starting positions was semi-randomly chosen every day. After 5 days of training, the platform was removed and a 24-hour probe trial was conducted. Mice were placed in the pool at starting position directly opposite from the platform's previous location and allowed to swim freely for 60 seconds and then removed and placed in a warming cage.

Novel Arm Y-Maze

Novel Arm Y-maze examines spatial working memory. Each arm of standard Y-maze was covered in different high contrast patterns. For training, mice were placed in the start arm of the maze with one of the choice arms blocked. Mice were allowed to freely explore the open arms for 7 minutes. The arm blocked during training was controlled for evenly within each treatment group to account for any bias to arm pattern or turning preference. Following completion of the training trial mice were removed and placed back in their home cage for 30 minutes. For the testing trial, mice were returned to the start arm with all arms open and allowed to freely explore for 7 minutes. In between all trials, the maze and walls were cleaned with 70% ethanol and dried to prevent odor cues from affecting performance.

Elevated Plus Maze

A standard mouse elevated plus maze (Stoelting Co.) was used to measure anxiety. The maze consists of four equal length arms which measured 35 x 5 cm and was raised 40cm above the ground. The two closed arms were enclosed with 15cm high walls. Mice were placed in the center of maze facing an open arm and allowed to freely explore the maze for 5 minutes in low light conditions (14 Lux). In between all trials, the arms and walls of the maze were cleaned with 70% ethanol and dried to prevent odor cues from affecting performance.

Tissue Processing

Immediately following perfusion, brains were quickly removed and hemispheres separated. The cerebellum was removed and then the right hemisphere was immediately flash-frozen in dry ice for subsequent biochemical analysis. The left hemisphere was drop-fixed in 4% paraformaldehyde for 48 hours at 4˚C. After 48 hours postfixation, the left hemispheres were transferred to 0.01M PBS and 0.02% NaN_3 for storage until sectioning. Brains were submerged in 30% sucrose for 48 hours prior to sectioning coronally on a freezing microtome at 40µm thickness. Free-floating sections were then placed back in 0.01M PBS and 0.02% NaN_3 for storage until used for histology.

Tissue Processing for Biochemical Analyses

Right hemispheres, previously frozen on dry ice and stored at -80˚ were microdissected and whole hippocampus was removed and homogenized in a solution of T-PER (Pierce) with phosphatase and protease inhibitor cocktails (Thermo Scientific & Roche) and then spun at 10,000 x g for 15 minutes at 4˚. The supernatant (soluble fraction) was extracted and stored at -80˚ for further biochemical analysis. For Aβ analysis the insoluble pellet was homogenized with 70% formic acid and spun at 100,000g for 1 hour. Supernatant (insoluble fraction) was removed and stored at -80˚ until further analysis. Prior to biochemical analyses volumes of insoluble fraction were neutralized with buffer containing 0.5M Tris-base, 0.25M Na_2HPO_4, and 5N NaOH.

Immunohistohemistry

Fluorescent immunohistochemical analysis followed previously described established protocols [Goldberg et al., 2015; Marsh et al., 2016]. Briefly, sections were incubated in primary antibodies overnight followed by detection with appropriate Alexa Fluor® conjugated secondary antibody (Invitrogen; Carlsbad, CA) and coverslipped using Fluoromount-G with or without DAPI (Southern Biotech).

Antibodies utilized were: Ku80 (human nuclei, Abcam; Cambridge, MA; ab80592 & ab79220), GFAP (Millipore; Billerica, MA; MAB360), GFAP (Dako; Carpinteria, CA; Z0334), Doublecortin (Santa Cruz Biotechnology; Dallas, TX; sc-8066), Olig2 (Millipore; MABN50), APC (CC-1) (Millipore; OP80-100UG), PSD95 (Abcam; ab13552), Vimentin (Dako; M0725), CD44 (Stem Cell Technologies; Vancouver, BC; #60068), S100β (Abcam; ab4066), LIN28 (Cell Signaling; Danvers, MA; #8706), NeuN (Millipore; ABN78), Ki67 (Abcam; ab16667). Negative controls were performed with omission of primary and secondary antibodies to verify the specificity of each antibody.

Confocal Microscopy and Immunohistochemical Analysis

Immunofluorescent sections were visualized and images captured using an Olympus FX1200 confocal microscope. To avoid non-specific bleed through each laser line was excited and detected independently. All images shown represent either single confocal *z*-slice or *z*-stacks. All image analyses were conducted by a blind observer using coded images

Analysis of HuCNS-SC differentiation was performed using Fluoview software (Olympus) by first overlaying images with 3x3 grid (~175µm x 175µm) followed by digital zoom to analyze one grid square at a time. Using both maximum projection images and orthogonal view the total number of Ku80+ and double-labeled HuCNS-SC were counted one grid square at a time. There was no significant difference between total number of Ku80+ cells counted between genotypes in either of the regions analyzed (data not shown) and average number of Ku80+ cells counted per region was ≥79.

High magnification confocal images of post-synaptic density (PSD95) immunolabeled sections were visualized with an Olympus FX1200 confocal microscope using the 40x oil objective with 5x digital zoom. 1-µm z-stack images were captured using 0.25µm step size in 4 randomly selected ROIs within the stratum oriens of the hippocampus. Post-synaptic puncta were counted using IMARIS (Bitplane; Concord,

MA) image analysis software using the "Spot" function. Identical settings used for spot analysis were for analysis of all images and all capture and analysis was performed by blind observer using coded images.

Light-level immunohistochemistry & Unbiased Stereological Quantification of HuCNS-SC Engraftment

To quantitatively measure HuCNS-SC engraftment following transplant every sixth coronal section was collected and incubated with an antibody against the human nuclear marker Ku80 (Abcam) overnight followed by incubation with biotin-conjugated secondary antibody. Antibody labeling was visualized using Vectastain Elite ABC kit (Vector Labs; Burlingame, CA) followed by 3,3'-diaminobenzidine (DAB) with Nickel Peroxidase (HRP) Substrate Kit (Vector Labs) before being mounted and coverslipped using DPX (DBH) mounting medium (VWR, Radnor, PA).

All unbiased stereological analysis was performed using Stereo Investigator software (MBF Bioscience; Williston, VT) on a Zeiss AXIO Imager.M2 microscope. Protocol for HuCNS-SC engraftment was adapted from previously published stereological protocols used for neuronal and stem cell quantification [Baglietto-Vargas et al., 2010; Ager et al., 2015].

Briefly, brain regions were outlined using the 2.5x/0.075 objective and all cell counts were performed using the 100x/1.4 objective. Briefly an optical fractionator probe was utilized to estimate the total number of engrafted HuCNS-SC. Stereological quantification was performed throughout the entire rostral/caudal extent of stem cell engraftment within the hippocampus and dorsal cortex. A counting frame of 50 x 50μm in a sampling grid of 350 x 350 μm was used for cell quantification. Guard zone height for both top and bottom was set at 3 μm with an optical dissector height of 10 μm. Using the optical fractionator formula, in which $N = 1/ssf.1/asf.1/hsf.\sum Q$, where ssf represents the section sampling fraction, asf is the sampling fraction, which is calculated by dividing the area sampled with the total area of the layer, hsf stands for the height sampling fraction, which is calculated by dividing the height sampled (10 μm in this study) with the section thickness, and $\sum Q$ is the total count of nuclei sampled for the entire area. The accuracy of the individual estimation was expressed by the total coefficient of error (CE) calculated using the CEs in each individual animal, with acceptable CE ranged between 0.02 and 0.09.

Multiplex ELISAs

Quantitative biochemical analysis of Aβ and BDNF were conducted using commercially available electrochemiluminescent multiplex assay system (Meso Scale Discovery (MSD); Gaithersburg, MD). Hippocampal lysates were analyzed using Human Aβ triplex for simultaenous measurement of Aβ38, Aβ40, and Aβ42 and a BDNF MSD ELISA assay was used to measure BDNF levels.

Independent histopathology examination by a contract research organization

To provide independent assessment of the HuCNS-SC-derived clusters located within the ventricles, both labeled and unlabeled sections were sent to Charles River, a contract research organization (CRO). Raw confocal image files for all images shown in Figure 6 and a software viewer were also provided. A Charles River veterinary pathologist performed standard Hematoxilin/Eosin staining of unlabeled sections and also examined a subset of the existing slides and images.